Nanocomposites constructed by rare-earth fluoride and silver bismuth sulfide nanorods for efficient cancer therapy

Kai Yan [1, a], Yingbing Liu [1, b], Guixia Liu [1, c]

[1] School of Chemistry and Environmental Engineering, Changchun University of Science and Technology, Changchun 130022, P.R.China

[a] 1940969436@qq.com, [b] liuyingbingfly@163.com, [c] liuguixia22@163.com,

Abstract. A novel photothermal therapy agent AgBiS2@PVP-NaYF4:Yb3+, Ho3+ multifunctional nanocomposite (NCs) was constructed. Through the research on the morphology, structure, and properties of the nanocomposite material, it was observed that the nanocomposites exhibited superior up-conversion luminescence (UCL) properties, remarkable photothermal conversion efficiency, and a highly effective photothermal cytotoxicity against tumor cells in vitro. Furthermore, the nanocomposites showed minimal cytotoxicity and excellent stability in MTT cell toxicity experiments. Consequently, the NCs represent a significant advancement for high-performance tumor photothermal therapy.

Keywords: Nanocomposite, Silver Bismuth Sulfide, Rare-earth, Photothermal Therapy.

1. Introduction

Cancer remains a major global public health threat, posing significant challenges in both understanding and treatment, and its treatment options include surgery, chemotherapy, and radiotherapy, however, these methods are often accompanied by side effects such as incomplete resection of cancer tissue, high recurrence rates, and drug resistance [1]. Photothermal therapy (PTT) utilizes nanomaterials to transform near-infrared light into heat energy, which induces cell membrane cracking, and digestive enzyme release and ultimately leads to cancer cell death through local high temperatures [2-3].

In recent years, chalcogenides have shown great application prospects in the fields of biomedicine due to their excellent properties, such as rich microstructures, suitable band gaps, and good semiconductor properties [4]. As a narrower-bandgap semiconductor, silver bismuth sulfide ($AgBiS_2$) has the advantages of high specificity, non-invasiveness, and precise temporal and spatial selectivity [5]. These materials can convert light energy into heat energy upon exposure to near-infrared irradiation, thereby generating sufficient thermal energy to induce tumor cell death. Therefore, it is particularly suitable as a photothermal conversion agents (PTCAs) in tumor PTT.

Rare earth up-conversion luminescent nanomaterials (UCNMs) are a new type of optical materials, that can emit short-wavelength visible light under the excitation of near-infrared light, and have unique multiphoton excitation characteristics [6,7]. Furthermore, it should be noted that UCNMs offer several advantages such as a larger light penetration depth, absence of background fluorescence, and minimal damage to biological tissues [8]. In biological imaging, UCNMs possess low imaging background signal, high resolution, and deep tissue penetration, which can be utilized for deep tissue imaging in visualized therapy [9,10]. Therefore, UCNMs are favored by more and more researchers in the field of bioimaging.

There have been several reports describing the combination of upconverting luminescent particles and chalcogenide to form multifunctional nanocomposites [6]. For instance, by uniformly assembling Bi_2Se_3 on the surface of UCNPs, the nanocomposites can be utilized for non-invasive UCL/CT dual-mode imaging for real-time dynamic monitoring under 808 nm near-infrared laser irradiation [11]. However, the system's photothermal efficiency needs further optimization and enhancement. Overall, integrating $AgBiS_2$ with narrower-bandgap and excellent photothermal properties excitation into UCNMs will be an inevitable trend in developing.

Herein, we first synthesized Bi_2S_3 nanorods by solvothermal method. Using Bi_2S_3 as a template

and reactant, $AgBiS_2$ nanorods were further prepared by the cation exchange method [12]. Subsequently, $AgBiS_2$ nanorods were combined with $NaYF_4$:Yb^{3+}, Ho^{3+} nanoparticles through PVP using a facile synthetic method to construct photothermal therapeutic $AgBiS_2$@PVP-$NaYF_4$:Yb^{3+}, Ho^{3+} multifunctional nanocomposites (NCs). This unique structure will further enhance the light absorption properties and good biocompatibility of $AgBiS_2$ nanorods. The synthesis procedure for NCs is illustrated in Scheme 1.

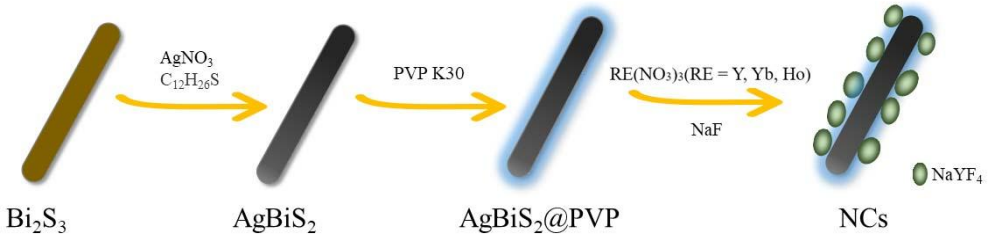

Scheme 1. Synthetic procedure illustration of the NCs.

2. Experimental

2.1 Chemicals

All raw materials without further purification used in our experiment include $Bi(NO_3)_3 \cdot 5H_2O$, $AgNO_3$, NaF, Thioacetamide (TAA), Ethylene glycol (EG), HNO_3, Y_2O_3, Yb_2O_3, Ho_2O_3 and Polyvinyl pyrrolidone (PVP). They were bought from Shanghai Macklin Biochemical Co. Ltd.

2.2 Synthesis of Bi_2S_3 and $AgBiS_2$ nanorods

Bi_2S_3 nanorods were synthesized using the hydrothermal method. Briefly, $Bi(NO_3) \cdot 5H_2O$ (1 mmol) was dissolved in ethylene glycol (35 mL) and stirred for 1 h. Then TAA (1.5 mmol) was added into the mixture and stirred for 1 h and calcined at 180°C for 16 h. $AgBiS_2$ nanorods were synthesized based on previous work with a slight modification [12]. The 0.25 mmol Bi_2S_3 nanorods were dissolved in 10 mL of oleylamine (solution A). 0.3 mmol $AgNO_3$ and 1 mL dodecyl mercaptan were dissolved in 10 mL oleylamine (solution B). Then solution B was dropped into solution A and stirred at 170 °C for 15 min.

2.3 Synthesis of NCs

First, $AgBiS_2$ nanorods (30 mg) were dissolved in ethanol (15 mL) and strongly stirred for 30 min. Subsequently, PVP (0.2 g) dissolved in ultrapure water (5 mL) was added dropwise to the dispersion and stirred magnetically for 16 h. Adding a mixed nitrate solution containing $Y(NO_3)_3$, $Yb(NO_3)_3$, and $Ho(NO_3)_3$ (molar ratio = 78:20:2) to the above dispersion. After stirring the mixed solution for 2 h. Subsequently, driping a solution of NaF (0.084 g) into the mixture. Then, the dispersion was stirred at 50 ℃ for 3 h.

2.4 Characterizations

The XRD patterns of the synthesized products were tested by X-ray diffraction instrument (RigakuD/max-RA). The UV-Vis-NIR absorption spectrum was measured by Shimadzu spectrophotometer (UV-2450). The morphology analyses of all samples were studied by JEOL JSM-7610F field emission SEM. The fluorescence spectra of the samples were tested by the F-7000 fluorescence spectrophotometer produced by Hitachi in Japan.

3. Results and discussion

3.1 Phase structure, morphology and composition

In order to explore the phase purity, crystal structure, morphology of the smaples, XRD and

SEM analyses were performed. As shown in Fig.1A, all diffraction peaks of Bi_2S_3 match with those of the orthorhombic phase Bi_2S_3 standard card (PDF#89-8964) in terms of intensity and position, confirming the phase purity of the synthesized Bi_2S_3 nanorods. As illustrated in Fig. 1D(a), $AgBiS_2$ match well with the standard card for $AgBiS_2$. This confirms that the synthesized $AgBiS_2$ is of pure phase. In Fig.1D(b), the diffraction peaks correspond to both $NaYF_4$ and $AgBiS_2$, confirming that the prepared NCs consist of both $AgBiS_2$ and $NaYF_4$:Yb^{3+}, Ho^{3+}. The SEM image (Fig. 1B) clearly reveals that Bi_2S_3 presents a uniform rod-shaped morphology. $AgBiS_2$ exhibits a uniform rod-like morphology(Fig. 1C), indicating that the morphology of the samples remain unchanged after the introduction of Ag^+. Furthermore, Fig. 1E reveals that the size of NCs has increased following the addition of $NaYF_4$, resulting in a notably rougher surface due to the coating of up-conversion nanoparticles on $AgBiS_2$. Fig. 1F shows the EDS spectrum of NCs, which indicates the presence of Bi, S, Ag, F, Na, Y, Yb, Ho, C, and O. It further confirmed the successful synthesis of NCs.

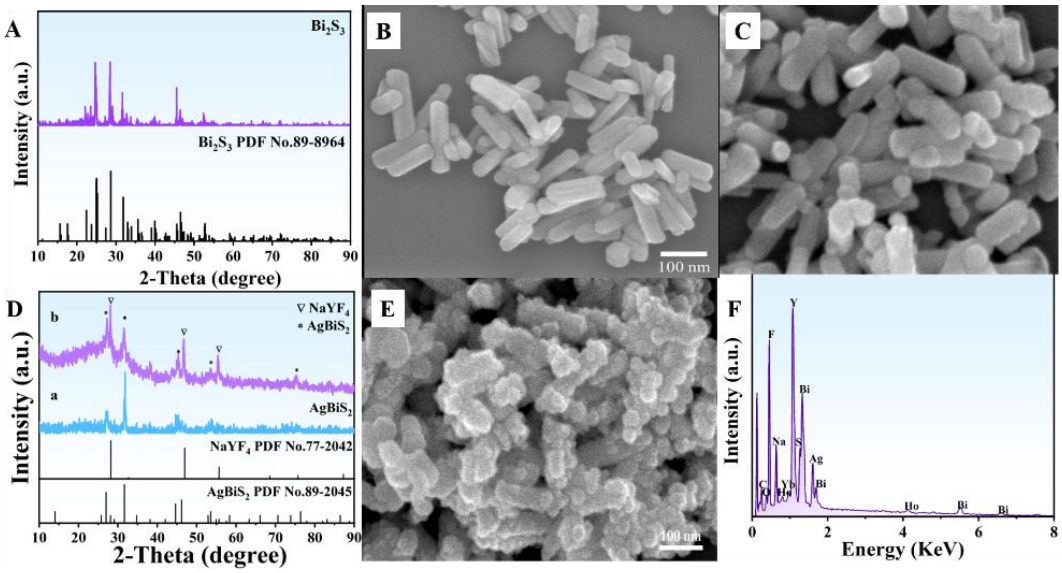

Fig. 1 XRD patterns of Bi_2S_3 (A) and $AgBiS_2$,NCs (D); SEM images of Bi_2S_3 (B); $AgBiS_2$ (C) and NCs (E); EDS spectrum of NCs (F).

3.2 Optical propertie

Fig. 2A and B shows the UV-Vis-NIR absorption spectra of Bi_2S_3, $AgBiS_2$, and NCs. As shown in Fig. 2A, $AgBiS_2$ exhibits significantly stronger absorption than Bi_2S_3 within the 350-850 nm range. Therefore, the concentration of defect sites of $AgBiS_2$ is higher, and the absorption for near-infrared light is stronger. From Fig. 2B, we can see that the NCs demonstrate a broad and continuous absorption band ranging from 400 to 800 nm. Furthermore, the absorption intensity of NCs increases with rising concentration, indicating that NCs possess superior near-infrared light absorption properties, which establishes a robust foundation for their applications in the biological field.

Fig. 2C showed that the up-conversion emission spectra of NCs and $NaYF_4$:Yb^{3+},Ho^{3+} nanoparticles have two characteristic emission peaks at 540 nm and 650 nm under 980 nm excitation, which are due to the $^5S_2/^5F_4 \rightarrow {}^5I_8$ and $^5F_5 \rightarrow {}^5I_8$ transitions of Ho^{3+}. Meanwhile, the addition of $AgBiS_2$ had no effect on the electronic transitions. However, the emission intensity of the NCs decreased slightly compared to that of the up-conversion nanoparticles. This indicates that $AgBiS_2$ effectively absorbed and converted the visible light emitted at 540 and 650 nm from the up-conversion process into heat. Combined with Fig. 2A, it is shown that NCs can absorb the visible light generated by the $NaYF_4$:Yb^{3+}, Ho^{3+} up-conversion process through the luminescence energy transfer mechanism. Therefore, the designed NCs can increase the absorption of NIR light. Fig. 2D illustrates the relationship between pump power and luminescence intensity for NCs. The

results show that the slopes of the NCs at 540 nm and 650 nm are 1.80 and 1.89 respectively, respectively. The two slope values are close to 2, indicating that the process is a two-photon process.

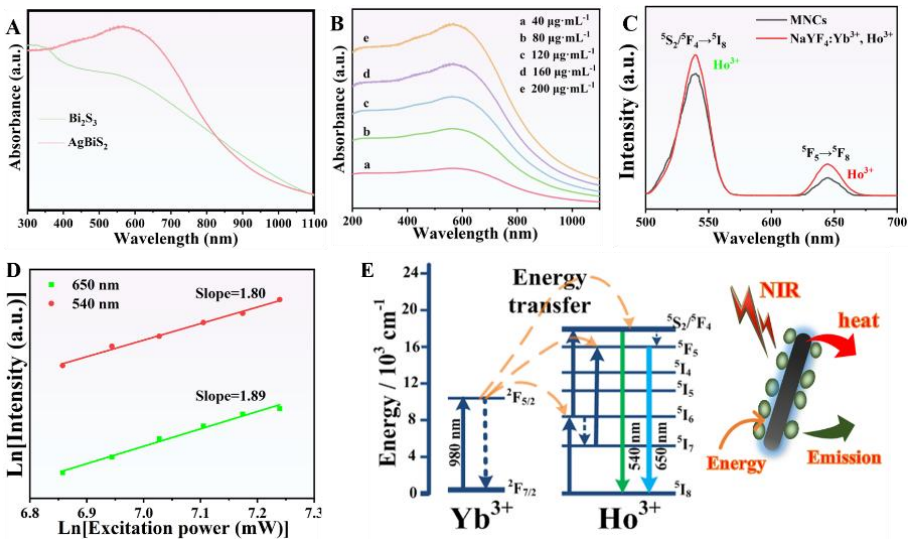

Fig. 2 UV-Vis-NIR absorption spectra of Bi_2S_3, $AgBiS_2$ (A) and NCs aqueous dispersions (B); Up-conversion emission spectra of NCs and $NaYF_4$:Yb^{3+}, Ho^{3+} under 980 nm excitation(C); Ln-Ln plot of UCL intensity and excitation power of NCs(D); schematic diagram of the energy transfer process of NCs(E).

3.3 Energy transfer process study

The energy conversion mechanism exhibited by NCs upon 980 nm laser irradiation in Fig. 2E. When illuminated by 980 nm light, Yb^{3+} ions absorb photons and transition from the $^2F_{7/2}$ state to the $^2F_{5/2}$ state, so that energy transfer occurs between Yb^{3+} ions and Ho^{3+} ions. Green emission at 540 nm, and red emission at 650 nm can be observed. As the luminescence of Ho^{3+} ions is quenched, and the energy is transferred to the $AgBiS_2$ nanorods, which will produce heat, the luminescence energy transfer phenomenon is caused.

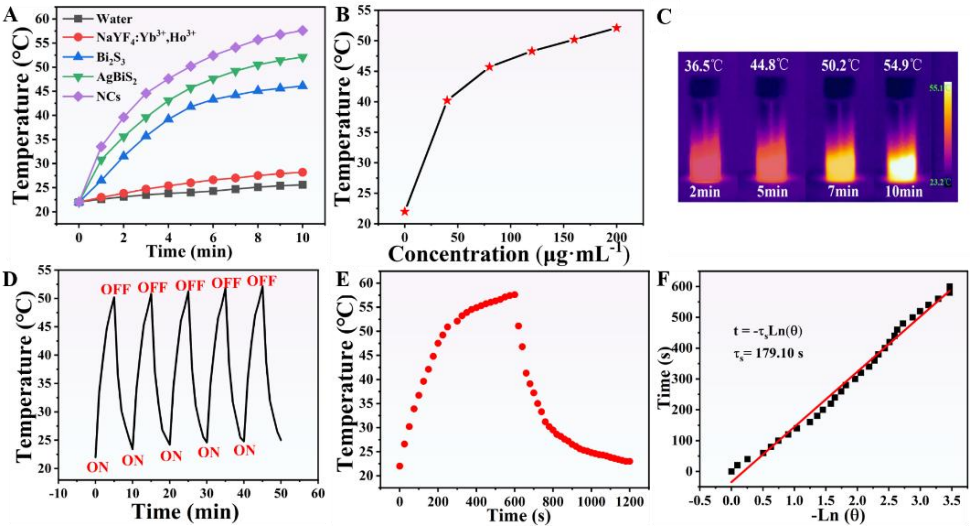

Fig. 3. Time-dependent temperature change of ultrapure water, dispersion of $NaYF_4$:Yb^{3+}, Ho^{3+}, Bi_2S_3, $AgBiS_2$ and NCs upon 1 W/cm^2 of 980 nm laser (A); NCs concentration-dependent temperature change (B); Infrared thermal images of NCs during irradiation (C); Photothermal stability of NCs under cyclic on/off irradiation conditions (D); Heating and cooling curves of NCs

solution under 980 nm laser on/off conditions (E); Linear regression curve obtained from the cooling process of NCs (F).

3.4 Photothermal performance analysis

The photothermal conversion performances of Bi_2S_3, $AgBiS_2$, and NCs were evaluated by monitoring the temperature changes in their aqueous solutions under 980 nm laser irradiation, maintaining identical concentration and power density. The time-temperature curves of ultrapure water, $NaYF_4$:Yb^{3+}, Ho^{3+}, Bi_2S_3, $AgBiS_2$ and NCs under NIR laser irradiation are shown in Fig. 3A. The temperatures of Bi_2S_3, $AgBiS_2$ and NCs rose quickly, from 22 °C to 46.1 °C, 52.1 °C and 57.6 °C. In contrast, the temperature of ultrapure water and $NaYF_4$:Yb^{3+}, Ho^{3+} increased gradually from 22 °C to 25.6 °C and 28.2 °C. The NCs exhibited a concentration-dependent photothermal conversion efficiency in Fig. 3B, even a low dose can enhance the temperature necessary to eliminate cancer cells (42 °C). As shown in Fig. 3C, the temperature can be increased with the irradiation times, the higher the temperature can achieve the more obvious the thermal imaging, thereby enhancing the dynamic tracking capability of the PTT process. From Fig. 3D, the NCs were irradiated for 5 min in each cycle followed by natural cooling. It can be seen that the NCs exhibited good photothermal stability throughout multiple irradiation cycles during the process of temperature increase and reduction.

Determine the photothermal conversion efficiency (η) utilizing the formula previously reported in the literature [13].

$$\eta = \frac{hS(T_{max}-T_{surr})-Q_0}{I(1-10^{-A_{808\,nm}})} \quad (1)$$

Combined systematic analysis of the data in Fig. 3E and F with formula (1) calculations, the NCs exhibited a photothermal conversion efficiency of 47.1%, Indicating that NCs demonstrate a markedly superior photothermal conversion efficiency compared to previously reported values for UCNPs-Bi_2Se_3 (29.9%) [11], $AgBiS_2$@CQDs (41.6%) [14] and $AgBiS_2$ hollow nanospheres (44.2%) [15]. It is further confirmed that NCs can significantly improve the photothermal performance under near-infrared laser irradiation. Therefore, NCs showing great potential to emerge as an efficient photothermal conversion reagent.

3.5 Cytotoxicity assay

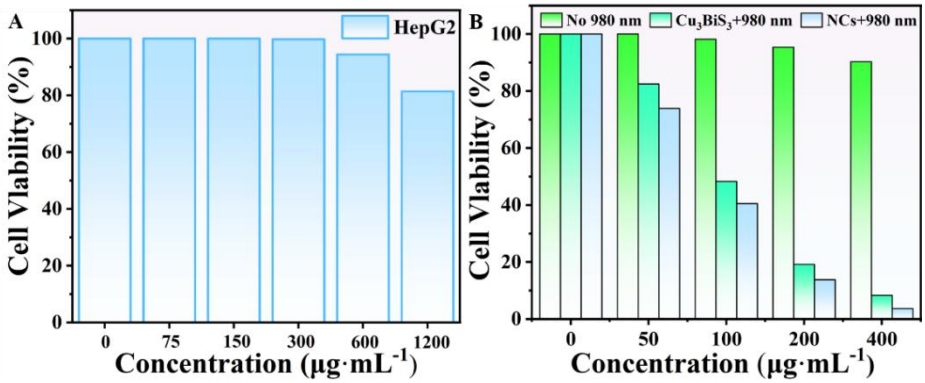

Fig. 4. Cell viability of HepG2 cells with $AgBiS_2$@PVP-$NaYF_4$:Yb^{3+},Ho^{3+} of various concentrations for 24 h (A); Cell viability of HepG2 cells incubated with different concentrations of Bi_2S_3, $AgBiS_2$ and NCs for 24 h and then irradiated with NIR laser for 10 min (B).

HepG2 cells were selected as the model cell line for MTT assay to evaluate the toxicity of NCs. In Fig. 4A, the cell survival rate can reach 81.5 % even at an NCs concentration of 1200 μg·mL-1. The data in Fig. 4B reveal that with increasing concentrations, the survival rate of HepG2 cells decreases after being exposed to a specific duration of NIR irradiation.AgBiS2 exhibits a greater killing rate compared to Bi2S3. At the same time, NCs have a higher kill rate than AgBiS2,

indicating that the energy transfer effect of NaYF4:Yb3+, Ho3+ also has a significant effect on improving the photothermal conversion ability. Notably, at a concentration of 400 $\mu g\ mL^{-1}$, the NCs induced a significant reduction in cell survival rate, plummeting to a mere 2.3%. Therefore, the MTT test shows that NCs have little toxicity to cells, which can be applied to the biological field.

4. Conclusions

In conclusion, we synthesized $AgBiS_2$@PVP-$NaYF_4$:Yb^{3+}, Ho^{3+} NCs through a simple liquid-phase method. The results show that the $AgBiS_2$ can significantly improve the photothermal performance under near-infrared laser irradiation. In addition, after $NaYF_4$:Yb^{3+}, Ho^{3+} is excited by 980 nm laser, it produces high-energy light emission, which further enhances the light absorption of NCs. Moreover, in vitro, cell photothermal conversion tests show that NCs have extremely low cytotoxicity and extremely high photothermal effects. Under near-infrared radiation, these properties enable the execution of high-performance photothermal therapy on tumor cells, which holds significant therapeutic potential for clinical localized cancer treatment.

Acknowledgements

This work was supported financially by the Science and Technology Development Planning Project of Jilin Province (20240101075JC).

Conflicts of Interest

The authors declare no conflicts of interest regarding the publication of this paper.

References

[1] Jin Longhai, Zhou Shijie, Zhang Tianqi, et al. A multi-functional cascade nanoreactor for remodeling tumor microenvironment to realize mitochondria dysfunction via ROS/Zn2+ ions overload. Small, 2025, 21(2): 2408639.

[2] Rozanova Nadejda, Zhang JinZhong. Photothermal ablation therapy for cancer based on metal nanostructures. Science in China Series B: Chemistry, 2009, 52(10): 1559-1575.

[3] Ma Gongcheng, Ding Qihang, Wang Yue, et al. Precision photothermal therapy at mild temperature: NIR-II imaging-guided, H2O2-responsive stealth nanobomb. Advanced Healthcare Materials, 2024: 2402767.

[4] Wang Chao, Sui Wenxia, Chen Wujun, et al. Recent advances in polysulfide-based prodrug nanomedicines for cancer therapy. Coordination Chemistry Reviews, 2024, 519: 216138.

[5] Yang Junlei, Yue Lihuan, Shen Bei, et al. Exploring the inhibitory effect of AgBiS2 nanoparticles on influenza viruses. International Journal of Molecular Sciences, 2023, 24(12): 10223.

[6] Yu Shaohua, Tu Datao, Lian Wei, et al. Lanthanide-doped near-infrared II luminescent nanoprobes for bioapplications. Science China-Materials. 2019, 62(8), 1071-1086.

[7] Zhang Ke, Wang Jingzhi, Peng Liqi, et al. UCNPs-based nanoreactors with ultraviolet radiation-induced effect for enhanced ferroptosis therapy of tumor. Journal of Colloid and Interface Science, 2023, 651: 567-578.

[8] Yang Miao, Gong Haijiang, Yang Dan, et al. Research progress on rare earth up-conversion and near-infrared II luminescence in biological applications. Chinese Chemical Letters, 2024, 35(2): 108468.

[9] Han Xuemin, Zhou Lei, Zhuang Hongjun, et al. Hybrid mesoporous MnO-upconversion nanoparticles for image-guided lung cancer spinal metastasis therapy. Acs Applied Materials & Interfaces. 2022, 14(16), 18031-18042.

[10] Zheng Xue, Du Yijing, Dang Zetao, et al. Biodegradable near-infrared-IIb rare-earth nanoprobe enables time-programmable neuroimaging. Advanced Functional Materials, 2024, 34(23): 2313278.

[11] Zhao Shuang, Tian Rongrong, Shao Baoqi, et al. UCNP–Bi2Se3 upconverting nanohybrid for upconversion luminescence and CT imaging and photothermal therapy. Chemistry A European Journal. 2020, 26(5), 1127-1135.

[12] Paul Sumana, Dalal Biswajit, Jana Rajkumar, et al. Enhanced photophysical properties of Bi2S3/AgBiS2 nanoheterostructures synthesized via Ag(I) cation exchange-mediated transformation of binary Bi2S3. The Journal of Physical Chemistry C. 2020, 124(23), 12824-12833.

[13] Hafner Jurgen. Ab-initio simulations of materials using VASP: density-functional theory and beyond. Journal of computational chemistry, 2008, 29(13): 2044-2078.

[14] Huo Dongliang, Liu Ting, Huang Kangkang, et al. AgBiS2@CQDs/Ti nanocomposite coatings for combating implant-associated infections by photodynamic/photothermal therapy. Biomaterials Advances, 2024, 158: 213763.

[15] Chen Benjin, Zhang Chenyang, Wang Wanni, et al. Ultrastable AgBiS2 hollow nanospheres with cancer cell-specific cytotoxicity for multimodal tumor therapy. ACS Nano. 2020, 14(11), 14919-14928.